# DOUBLE DIFFUSIVE FREE CONVECTION IN A PACKED BED SQUARE ENCLOSURE BY USING LOCAL THERMAL NON-EQUILIBRIUM (LTNE) MODEL

***Ahmed N. Mehdy***
*Assistant Lecturer*
*Department of Mechanical Engineering*
*Engineering college*

## ABSTRACT

In the present study, free convection heat and mass transfer of fluid in a square packed bed enclosure is numerically investigated. For the considered geometrical shape, the left vertical wall of enclosure was assumed to be kept at high temperature and concentration while the opposite wall was kept at low temperature and concentration with insulating both the top and bottom walls of enclosure. The Brinkman–Forchheimer extended Darcy model was used to solve the momentum equations, while the energy equations for fluid and solid phases were solved by using the local thermal non-equilibrium (LTNE) model. Computations are performed for a range of the Darcy number from $10^{-5}$ to $10^{-1}$, the porosity from ***0.5*** to ***0.9***, and buoyancy ratio from ***-15*** to ***15***. The results showed that both the buoyancy ratio and the packed bed characteristics have significant effect on each one of the flow field, heat transfer and mass transfer.

**الخلاصة**

خلال الدراسة الحالية، انتقال الحرارة والكتلة بالحمل الحر خلال طبقات محشوة في تجويف مربع تم دراسته عددياً. للنموذج الهندسي المفترض، تم اعتبار الجدار العمودي الأيسر للتجويف محفوظ عند درجة حرارة وتركيز مرتفعين بينما الجدار المقابل قد حُفظ عند درجة حرارة وتركيز واطئين مع عزل كل من الجدارين العلوي والسفلي. تم استخدام نموذج برنكمان- فورشماير المشتق من نموذج دارسي في حل معادلات الزخم، بينما تم حل معادلات الطاقة لكل من الطورين المائع والصلب باستخدام نموذج عدم الاتزان الحراري الموقعي (LTNE). لقد أنجزت الحسابات لمدى رقم دارسي من $10^{-5}$ إلى $10^{-1}$، المسامية من ***0.5*** إلى ***0.9***، ونسبة الطفو من ***-15*** إلى ***15***، أظهرت النتائج بأن كلاً من نسبة الطفو وخصائص الطبقات المحشوة تمتلكان تأثيراً مهماً على كل من حقل الجريان، انتقال الحرارة وانتقال الكتلة.

**Keywords: Double Diffusive, Free Convection, Packed Bed, Local thermal non-equilibrium.**

## INTRODUCTION

Double-diffusive convection or thermosolutal convection is generally referred to a fluid flow generated by buoyancy effects due to both temperature and solutal concentration gradients. This type of flow is encountered in natural and technological applications. Such applications include the growth of crystals, solar energy systems, welding processes, thermal insulations.

The term double diffusive-convection is now widely accepted for all processes which involve simultaneous thermal and solutal concentration gradients and provides an explanation for a number of natural phenomena. Because of the coupling between the fluid velocity field and the diffusive (thermal and solutal concentration) fields, double-diffusive convection is more complex than the convection flow which is associated with a single diffusive scalar, and many different behaviours may be expected. Such double-diffusive processes occur in many fields, including chemical engineering (drying, cleaning operations, evaporations, condensation, sublimation, deposition of thin films, energy storage in solar ponds, roll-over in storage tanks containing liquefied natural gas, solution mining of salt caverns for crude oil storage, casting of metal alloys and photosynthesis), oceanography (melting and cooling near ice surfaces, sea water intrusion into freshwater lakes and the formation of layered or columnar structures during crystallisation of igneous intrusions in earth's crust), geophysics (dispersion of dissolvent materials or particulate matter in flows), etc. A clear understanding of the nature of the interaction between thermal and mass or solutal concentration buoyancy forces is necessary in order to control these processes. **(Chaudhary and Jain, 2007)** studied the MHD flow past an infinite vertical oscillating plate through porous medium with the presence of free convection and mass transfer analytically by using Laplace-transform technique. **(Mohamed, 2009)** analyzed the double-diffusive convection-radiation interaction for the unsteady MHD flow over a semi-infinite vertical moving porous plate embedded in a porous medium in the presence of thermal & solutal diffusion and heat generation. A numerical study of the unsteady free convection and mass transfer flow of an electrically conducting fluid past an infinite vertical porous plate in the presence of a transverse magnetic field was presented by **(Shariful et. al. , 2005)**. **(Bukhari, 2003)** applied a linear stability analysis, using the spectral Chebyshev polynomial method, to obtain numerically the solution of a multi-layer system consisting of the finger convection onset in a fluid layer overlying a porous layer. **(Saha and Hossain, 2004)** studied numerically the laminar doubly diffusive free convection flows along an isothermal vertical finite plate immersed in a stable thermally stratified fluid by using an implicit finite difference method and local non-similarity method. **(Hajri et. al. , 2007)** presented a numerical simulation for the steady double-diffusive natural convection in a triangular cavity by using equal finite elements method. A numerical study was presented from **(Mamou et. al. , 2001)** for the unsteady double-diffusive convection in a two-dimensional horizontal confined enclosure by using the finite element technique. **(Masuda et. al. , 2002)** presented a numerical simulation by using finite differences

method for the unsteady two-dimensional double-diffusive convection in porous rectangular enclosure. After that, **(Masuda et. al. , 2008)**s studied the peculiar oscillating convection which is observed when two-dimensional double-diffusive convection in porous medium is analyzed numerically. **(Khanafer and Vafai, 2002)** presented a numerical study of mixed-convection heat and mass transport in a lid-driven square enclosure filled with a non-Darcian fluid-saturated porous medium by using the finite volumes technique. **(Rahli and Bouhadef, 2004)** studied numerically the double-diffusive natural convection in a partially porous square enclosure with the presence of inclination effect by using the control volume method and the power law scheme. **(Wang et. al., 2007)** presented a numerical investigation of natural convection of fluid (without mass transfer) in an inclined square enclosure filled with porous medium and submitted to a strong magnetic field by using (LTNE) model. However, the buoyancy force due to the double-diffusive effect has received more attention in the literature. But all the previous studies which deal with the double-diffusive convection in porous mediums assume that the porous medium in thermo dynamical equilibrium with the fluid which flow inside it, except **(Wang et. al., 2007)** which studied the pure convection without mass transfer in the presence of heat transfer between the fluid and the porous media. The present study gives more attention to the interaction between the effect of the double-diffusive convection and the effect of heat transfer between the porous medium and the fluid which flows inside it.

## MATHEMATICAL MODEL

### Geometrical Shape of Studied Problem

The schematic view of the studied problem is shown in Fig.1. The square enclosure has a side length (a) and it is filled with a saturated packed bed. The left vertical wall of the square enclosure is kept at high temperature and concentration while the opposite wall is kept at low temperature and concentration, finally, the horizontal walls are insulated.

### Governing Equations

In the model development, the following assumptions are adopted; the working fluid has a Prandtl number ***Pr=0.71*** and assumed to be incompressible and Newtonian fluid, no phase change occurs and the process is in a steady state, the thermo physical properties of the fluid are assumed to be constant except the density variation in the buoyancy force, which is approximated according to the Boussinesq approximation. This variation, due to both temperature and solutal concentration gradients can be described as follow **(Khanafer and Vafai, 2002**);

$$\rho=\rho_0\left[1-\beta_T\left(T-T_L\right)-\beta_C\left(c-c_L\right)\right] \qquad (1)$$

Where $\boldsymbol{\beta_T}$ and $\boldsymbol{\beta_C}$ are the coefficients of the thermal and solutal expansions, which are defined as follow **(Khanafer and Vafai, 2002)**;

$$\beta_T=-\frac{1}{\rho_0}\left(\frac{\partial\rho}{\partial T}\right)_{p,c} \quad \& \quad \beta_C=-\frac{1}{\rho_0}\left(\frac{\partial\rho}{\partial c}\right)_{p,T} \qquad (2)$$

The Brinkman–Forchheimer extended Darcy model is used to solve the momentum equations while the energy equations for fluid and solid phases are solved with the local thermal non-

equilibrium (LTNE) model. Thus, the governing equations for the present study will take the following forms as in **(Amiri and Vafai, 1998)** and **(Khanafer and Vafai, 2002)**;

- Continuity equation

$$\frac{\partial u}{\partial x}+\frac{\partial v}{\partial y}=0 \qquad (3)$$

- Momentum equations

$$\frac{\rho_f}{\varepsilon^2}\left(u\frac{\partial u}{\partial x}+v\frac{\partial u}{\partial y}\right)= -\frac{\partial p}{\partial x}+\frac{\mu_f}{\varepsilon}\left(\frac{\partial^2 u}{\partial x^2}+\frac{\partial^2 u}{\partial y^2}\right)-\frac{\mu_f}{K}u+\frac{F\rho_f|\vec{u}|u}{\sqrt{K}} \qquad (4)$$

$$\frac{\rho_f}{\varepsilon^2}\left(u\frac{\partial v}{\partial x}+v\frac{\partial v}{\partial y}\right)=-\frac{\partial p}{\partial y}+\frac{\mu_f}{\varepsilon}\left(\frac{\partial^2 v}{\partial x^2}+\frac{\partial^2 v}{\partial y^2}\right) +\rho_f g\left[\beta_T(T_f-T_I)+\beta_C(c-c_I)\right]-\frac{\mu_f}{K}v+\frac{F\rho_f|\vec{u}|v}{\sqrt{K}} \qquad (5)$$

- Fluid phase energy equation

$$\rho_f\, cp_f\left(u\frac{\partial T_f}{\partial x}+v\frac{\partial T_f}{\partial y}\right)= k_{feff}\left(\frac{\partial^2 T_f}{\partial x^2}+\frac{\partial^2 T_f}{\partial y^2}\right)+a_{sf}\, h_{sf}\left(T_s-T_f\right) \qquad (6)$$

- Solid phase energy equation

$$k_{seff}\left(\frac{\partial^2 T_s}{\partial x^2}+\frac{\partial^2 T_s}{\partial y^2}\right)+a_{sf}\, h_{sf}\left(T_f-T_s\right)=0 \qquad (7)$$

- Solutal concentration equation

$$u\frac{\partial c}{\partial x}+v\frac{\partial c}{\partial y}=D\left(\frac{\partial^2 c}{\partial x^2}+\frac{\partial^2 c}{\partial y^2}\right) \qquad (8)$$

The geometric function ***F***, specific surface area of the packed bed $a_{sf}$ and the fluid-to-solid heat transfer coefficient in a packed bed $h_{sf}$ are determined as suggested by **(Amiri and Vafai, 1998)**;

$$F=\frac{1.75}{\sqrt{150\,\varepsilon^3}} \qquad (9.a)$$

$$a_{sf}=\frac{6(1-\varepsilon)}{d_p} \qquad (9.b)$$

$$h_{sf}=k_f\left[2+1.1\,\mathrm{Pr}^{1/3}\left(\frac{\rho_f|\vec{u}|d_p}{\mu_f}\right)^{0.6}\right] \qquad (9.c)$$

where the sphere particle diameter ***dp*** can be computed as follow **(Amiri and Vafai, 1998)**;

$$d_p=(1-\varepsilon)\sqrt{\frac{150\;K}{\varepsilon^3}} \qquad (9.d)$$

while the effective thermal conductivity $k_{feff}$ and $k_{seff}$ in fluid and solid phase energy equations and the mean thermal diffusivity $\alpha_m$ can be computed as follow **(Wang et. al. , 2007)**;

$$k_{feff}=\varepsilon\;k_f \qquad (10.a)$$

$$k_{seff}=(1-\varepsilon)\;k_s \qquad (10.b)$$

$$\alpha_m=\frac{k_{feff}+k_{seff}}{\rho_f\;cp_f} \qquad (10.c)$$

Now we introduce the following non-dimensional quantities and parameters as in **(Khanafer and Vafai, 2002)** and **(Wang et. al. , 2007)**;

$$\left.\begin{aligned} X &= \frac{x}{a}, \quad Y = \frac{y}{a} \\ U &= \frac{a\,u}{\alpha_m}, \quad V = \frac{a\,v}{\alpha_m}, \\ P &= \frac{p\,a^2}{\rho_f\,\alpha_m{}^2} \\ \theta_f &= \frac{(T_f - T_L)}{(T_H - T_L)}, \\ \theta_s &= \frac{(T_s - T_L)}{(T_H - T_L)}, \\ C &= \frac{(c - c_L)}{(c_H - c_L)} \end{aligned}\right\} \qquad (11.a)$$

$$\left.\begin{aligned} \mathrm{Pr} &= \frac{\mu_f\, cp_f}{k_{feff} + k_{seff}} = \frac{\nu_f}{\alpha_m} \\ , \quad Gr_T &= \frac{g\,a^3\,\beta_T\,(T_H - T_L)}{\nu_f^2} \\ Gr_C &= \frac{g\,a^3\,\beta_C\,(c_H - c_L)}{\nu_f^2}, \\ Da &= \frac{K}{a^2}, \quad Sc = \frac{\nu_f}{D} \\ N &= \frac{\beta_C\,(c_H - c_L)}{\beta_T\,(T_H - T_L)} = \frac{Gr_C}{Gr_T}, \\ \Lambda &= \frac{k_{feff}}{k_{seff}}, \quad \xi = \frac{a_{sf}\,h_{sf}\,a^2}{k_{feff}} \end{aligned}\right\} \qquad (11.b)$$

By substituting **eqs.(11.a & 11.b)** in **eqs.(3, 4, 5, 6, 7 & 8)**, we get the dimensionless forms of governing equations as follow;

$$\frac{\partial U}{\partial X} + \frac{\partial V}{\partial Y} = 0 \qquad (12)$$

$$\frac{1}{\varepsilon^2}\left(U\frac{\partial U}{\partial X} + V\frac{\partial U}{\partial Y}\right) = -\frac{\partial P}{\partial X} + \frac{\mathrm{Pr}}{\varepsilon}\left(\frac{\partial^2 U}{\partial X^2} + \frac{\partial^2 U}{\partial Y^2}\right) - \frac{\mathrm{Pr}}{Da}U - \frac{F\left|\vec{U}\right|U}{\sqrt{Da}} \qquad (13)$$

$$\frac{1}{\varepsilon^2}\left(U\frac{\partial V}{\partial X} + V\frac{\partial V}{\partial Y}\right) = -\frac{\partial P}{\partial Y} + \frac{\mathrm{Pr}}{\varepsilon}\left(\frac{\partial^2 V}{\partial X^2} + \frac{\partial^2 V}{\partial Y^2}\right) + \mathrm{Pr}^2\,Gr_T\left(\theta_f + N\,C\right) - \frac{\mathrm{Pr}}{Da}V - \frac{F\left|\vec{U}\right|V}{\sqrt{Da}} \qquad (14)$$

$$\left(1 + \Lambda^{-1}\right)\left(U\frac{\partial \theta_f}{\partial X} + V\frac{\partial \theta_f}{\partial Y}\right) = \left(\frac{\partial^2 \theta_f}{\partial X^2} + \frac{\partial^2 \theta_f}{\partial Y^2}\right) + \xi\,(\theta_s - \theta_f) \qquad (15)$$

$$0 = \left(\frac{\partial^2 \theta_s}{\partial X^2} + \frac{\partial^2 \theta_s}{\partial Y^2}\right) + \Lambda\,\xi\,(\theta_f - \theta_s) \qquad (16)$$

$$U\frac{\partial C}{\partial X} + V\frac{\partial C}{\partial Y} = \frac{\mathrm{Pr}}{Sc}\left(\frac{\partial^2 C}{\partial X^2} + \frac{\partial^2 C}{\partial Y^2}\right) \qquad (17)$$

By using the (stream function-vorticity) formulation we will reduce the dependent variables to only five variables by differentiating **eq.(13)** with respect to (Y) and differentiating **eq.(14)** with respect to (X), after that we subtract the first of the two resulted equations from the second to eliminate the pressure terms from the momentum equations, thus, **eqs.(12, 13 & 14)** will be transformed to the following equations;

$$\frac{\partial^2 \psi}{\partial X^2} + \frac{\partial^2 \psi}{\partial Y^2} = -\omega \qquad (17)$$

$$U\frac{\partial \omega}{\partial X} + V\frac{\partial \omega}{\partial Y} = \varepsilon\,\mathrm{Pr}\left(\frac{\partial^2 \omega}{\partial X^2} + \frac{\partial^2 \omega}{\partial Y^2}\right) + \varepsilon^2\left[\mathrm{Pr}^2 Gr_T\left(\frac{\partial \theta_f}{\partial X} + N\frac{\partial C}{\partial X}\right) - \left(\frac{\mathrm{Pr}}{Da} + \frac{F\left|\vec{U}\right|}{\sqrt{Da}}\right)\omega - \frac{F}{\sqrt{Da}}\left(V\frac{\partial \left|\vec{U}\right|}{\partial X} - U\frac{\partial \left|\vec{U}\right|}{\partial Y}\right)\right] \qquad (18)$$

where $\psi$ and $\omega$ are the (stream function & vorticity) respectively, and they are defined as follow;

$$U = \frac{\partial \psi}{\partial Y} \;\&\; V = -\frac{\partial \psi}{\partial X} \qquad (19.a)$$

$$\omega = \frac{\partial V}{\partial X} - \frac{\partial U}{\partial Y} \qquad (19.b)$$

After getting the final values of all dependent variables in the flow field, calculations will be made for local and mean Nusselt and Sherwood numbers, where the local Nusselt and Sherwood numbers at the hot wall can be found as in **(Wang et. al. , 2007)** and **(Khanafer and Vafai, 2002)**;

$$Nu_l = \varepsilon\left(\left.\frac{\partial \theta_f}{\partial X}\right|_{X=0} + \Lambda^{-1}\left.\frac{\partial \theta_s}{\partial X}\right|_{X=0}\right) \qquad (20.a)$$

$$Sh_l = \left.\frac{\partial C}{\partial X}\right|_{X=0} \qquad (20.b)$$

**Boundary Conditions**

The hydrodynamic boundary conditions for the present problem at all enclosure walls will obey to the non-slip condition, while the thermal and solutal boundary conditions are (the left side wall was kept at high temperature and solutal concentration, the right side wall was kept at low temperature and solutal concentration and finally each one of the top and bottom walls were kept insulated), thus the boundary conditions will be as follow;

$$\left.\begin{array}{l} U=0, V=0, \theta_f=\theta_s=C=1 \\ at\ X=0; \\ U=0, V=0, \theta_f=\theta_s=C=0 \\ at\ X=1; \\ U=0, V=0, \dfrac{\partial \theta_f}{\partial Y}=\dfrac{\partial \theta_s}{\partial Y}=\dfrac{\partial C}{\partial Y}=0 \\ at\ Y=0\,\&\,1 \end{array}\right\} \qquad (21)$$

**NUMERICAL SOLUTION**

The governing equations for $\psi$, $\omega$, $\theta_f$, $\theta_s$ & $C$ can be written in a common form for the (convection-diffusion) problem as follow **(Versteeg and Malalasekera, 1995)**;

$$\frac{\partial}{\partial X_i}\left(\rho u_i \Phi\right) = \frac{\partial}{\partial X_i}\left(\Gamma \frac{\partial \Phi}{\partial X_i}\right) + S \qquad (22)$$

where the general scalar $\Phi$ stands for any one of the dependent variables under consideration, the diffusion coeffecient $\Gamma$ and the source term $S$ in the cartesian form are listed below for each governing equation;

- Stream function equation

$$\Phi = \psi,\ \Gamma = 1,\ S = \omega \qquad (23.a)$$

- Vorticity equation

$$\Phi = \omega,\ \Gamma = \varepsilon \Pr,\ S = \varepsilon^2\left[\Pr^2 Gr_T\left(\frac{\partial \theta_f}{\partial X} + N\frac{\partial C}{\partial X}\right) - \left(\frac{\Pr}{Da} + \frac{F\left|\vec{U}\right|}{\sqrt{Da}}\right)\omega - \frac{F}{\sqrt{Da}}\left(V\frac{\partial\left|\vec{U}\right|}{\partial X} - U\frac{\partial\left|\vec{U}\right|}{\partial Y}\right)\right] \qquad (23.b)$$

- Fluid phase energy equation

$$\Phi = \theta_f,\ \Gamma = \frac{1}{1+\Lambda^{-1}},\ S = \frac{\xi(\theta_s - \theta_f)}{1+\Lambda^{-1}} \qquad (23.c)$$

- Solid phase energy equation

$$\Phi = \theta_s,\ \Gamma = 1,\ S = \Lambda\,\xi(\theta_f - \theta_s) \qquad (23.d)$$

- Solutal concentration equation

$$\Phi = C,\ \Gamma = \frac{\Pr}{Sc},\ S = 0 \qquad (23.e)$$

**T**he numerical solution of the governing equations will be made according to the finite volume method to transform the governing equations from partial differential form to discrete algebraic form, this method is based on principle of dividing the flow field to a number of volume elements, each one of them is called (control volume), after that a discretization process **(Versteeg and Malalasekera, 1995)** was carried out by integrating **eq.(22)** (of the general conservation) over a control volume element, where this equation will be as follow;

$$a_P \Phi_P = a_E \Phi_E + a_W \Phi_W + a_N \Phi_N + a_S \Phi_S + S_u \qquad (24)$$

where;

$$a_P = a_E + a_W + a_N + a_S - S_P \qquad (25)$$

the source coefficients $S_u$ and $S_p$ represent the source terms of the discrete equation and their values for each governing equation are listed as follow;

- For the stream function equation

$$\left.\begin{aligned} S_u &= \omega \\ S_p &= 0 \end{aligned}\right\} \qquad (26.a)$$

- For the vorticity equation

$$\left.\begin{aligned} S_u &= \varepsilon^2 \left[ \begin{aligned} &\mathrm{Pr}^2 Gr_T \left( \frac{\partial \theta_f}{\partial X} + N \frac{\partial C}{\partial X} \right) - \\ &\frac{F}{\sqrt{Da}} \left( V \frac{\partial |\vec{U}|}{\partial X} - U \frac{\partial |\vec{U}|}{\partial Y} \right) \end{aligned} \right] \\ S_p &= -\varepsilon^2 \left( \frac{\mathrm{Pr}}{Da} + \frac{F|\vec{U}|}{\sqrt{Da}} \right) \end{aligned}\right\} \qquad (26.b)$$

- Fluid phase energy equation

$$\left.\begin{aligned} S_u &= \frac{\xi \, \theta_s}{1 + \Lambda^{-1}} \\ S_p &= -\frac{\xi}{1 + \Lambda^{-1}} \end{aligned}\right\} \qquad (26.c)$$

- Solid phase energy equation

$$\left.\begin{aligned} S_u &= \Lambda \, \xi \, \theta_f \\ S_p &= -\Lambda \, \xi \end{aligned}\right\} \qquad (26.d)$$

- Solutal concentration equation

$$\left.\begin{aligned} S_u &= 0 \\ S_p &= 0 \end{aligned}\right\} \qquad (26.e)$$

A computational program was written in Fortran-90 language to compute the values of the required variables, The discretized algebraic equations are solved by the tri-diagonal matrix algorithm (TDMA). The used mesh size is ***(60×60)***. Relaxation factors of about ***(0.7–0.9)*** are used for all dependent variables, Convergence was measured in terms of the maximum change in each variable during an iteration where the maximum change allowed for convergence check was $10^{-6}$.

## RESULTS AND DISCUSSION

All solution were carried out for solution of ***(Pr=0.71 & Sc=0.25)*** at $Gr_T = 10^5$, where the numerical code which is used in the present investigation has been carried out for number of simulations for a wide range of controlling parameters such as buoyancy ratio, Darcy number, and porosity of the packed bed. **Figs.(2 - 9)** show the effect of buoyancy ratio for different values of ***(-15≤N≤15)*** on the stream function, fluid phase temperature and solutal concentration contours respectively at $Da=10^{-1}$ and ***ε=0.9***. **Figs.[(2.a), (2.b) & (2.c)]** represent these contours for the case of single diffusing effect at ***N=0***, where there is only thermal diffusing without solutal diffusing. It is clear from the stream function contour at ***N=0*** and as a result of the thermal buoyancy effect, the fluid at the left-hand side hot wall will be lighter than in other locations while the fluid at the right-hand side cold wall will be heavier than in other locations, so, the fluid particles move upward

along the hot wall while they move downward along the cold wall, and thus, the flow will take the direction of clockwise. The fluid phase temperature contour at ***N=0*** indicates that the temperature levels will decrease gradually from the hot wall towards the cold wall, where the hot fluid rises up along the left-hand side hot wall and descends along the right-hand side cold wall because of the thermal buoyancy effect. Finally the solutal concentration contour at ***N=0*** indicates that the solutal concentration will be maximum at the hot regions and decreases gradually with the decrease of the fluid phase temperature. After that, and with increasing the positive buoyancy ratio ***N>0*** as shown in **Figs.(3, 4 & 5)** which represent the cases at ***N=5, 10 & 15***, and as it is clear from these figures, the solutal buoyancy force which increases with the buoyancy ratio will cooperate with the thermal buoyancy and they'll drive the flow in the same direction to form a cooperator flow, where the stream function levels will increase with increasing in positive buoyancy ratio because of the increase of the total buoyancy force due to both the thermal and solutal diffusing, while as it is shown from the contours of fluid phase temperature, its distribution will keep on the same previous behavior, but the gradients will be stronger than them at ***N=0*** and increase directly with increase of the buoyancy ratio, also a similar behavior to the fluid temperature distribution will appear in the contours of the solutal concentration, but their gradients will be relatively less than the gradients of the fluid phase contours because of the absence of internal transference sources as it is clear from **eq.(23.e)**. **Figs.(6, 7, 8, 9)** the cases of negative buoyancy ratio ***N<0***, where the negative value of buoyancy ratio means that the value of solutal expansion coefficient $\beta_C$ is negative too, and as it is clear from the density definition in **eq.(1)**, the fluid density will increase with increase of the solutal concentration, and as a result, the flow begins to reverse its direction, So, the flow case at ***N=-1*** as it is shown in **Figs.[(6.a), (6.b) & (6.c)]** represents a conversion point in the flow direction from clockwise to counterclockwise as it is shown from the stream function distribution at ***N=-1***, where the clockwise main central vortex which formed at each of the previous cases of positive buoyancy ratio will divide into two main vortices in two opposite directions, also the distribution of both the fluid phase temperature and the solutal concentration at ***N=-1*** will begin to change their directions and their gradient will be at the minimum levels at this case. With increasing the value of negative buoyancy ratio as it is shown in **Figs.[(7.a), (7.b) & (7.c)]** which represent the flow case at ***N=-5***, the negative solutal buoyancy effect will be greater than the thermal buoyancy effect, and as a result of the total negative buoyancy effect, the fluid at the hot wall will be heavier than it in other locations while the fluid at the cold wall will be lighter than it in other locations, so, the fluid particles move downwards along the hot wall while they move upwards along the cold wall, and thus, the flow will take the direction of counterclockwise. The fluid phase temperature contour at ***N=-5*** indicates that the temperature levels will decrease gradually from the hot wall towards the cold wall, where the hot fluid descends downwards along the hot wall and rises up along the cold wall because of the large negative effect of solutal buoyancy. Finally the solutal concentration contour at ***N=-5*** indicates that the solutal concentration will be maximum at the hot regions and decreases gradually with the decrease of the fluid phase temperature. **Figs.(8 & 9)** represent the flow case at ***N=-10 & -15*** respectively, and as it is clear that the levels of counterclockwise stream function will increase

with the increase of negative value of buoyancy ratio, while the fluid phase temperature and solutal concentration keep the same previous behaviours but their gradients increase with the increase of negative value of buoyancy ratio. **Figs.(10.a & 10.b)** indicate the variation of velocity components with buoyancy ratio at the intermediate vertical and horizontal locations respectively for $Da=10^{-1}$ and $\varepsilon=0.9$, where as it is shown in **Fig.(10.a)** the horizontal velocity component at the positive values of buoyancy ratio will direct to the right in top half of the enclosure while it will be in opposite direction in the bottom half of the enclosure because of the positive total buoyancy effect, while we'll note the conversion in flow direction nearly at $N=-1$ where the horizontal velocity begins to reverse its direction as it happens when the value of negative buoyancy ratio becomes $N<-1$, also as it is shown in **Fig.(10.b)**, the vertical velocity component at the positive values of buoyancy ratio will direct upwards in the left half of the enclosure while it will be in opposite direction in the right half of the enclosure because of the positive total buoyancy effect, where it begins to reverse its direction at the negative buoyancy ratios of $N<-1$. **Fig.(11)** represents the variation of local Nusselt number with buoyancy ratio at $Da=10^{-1}$ and $\varepsilon=0.9$, where it is clear that the value of local Nusselt number at $N\geq 0$ will be maximum at the bottom of the left-hand vertical wall and it descends gradually with rising to the wall top because the temperature gradient will be very strong at the bottom and it decreases gradually to the top, also it is clear the increasing in the local Nusselt number levels with the increase of positive buoyancy ratio, while the minimum levels of it will be at $N=-1$ because the temperature gradients were minimum at that buoyancy ratio value, also at $N<-1$ it is clear that the value of local Nusselt number will be maximum at the top of the hot wall and it descends gradually with dropping down to the wall bottom because the temperature gradient will be very strong at the top and it decreases gradually to the bottom. **Fig.(12)** represents the variation of local Sherwood number with buoyancy ratio (which is analog to Nusselt number in heat transfer, where it gives an indication to the rate of mass transfer through the solution which happens by solutal concentration difference), where it is clear that the distribution of local Sherwood number will be similar to the distribution of local Nusselt number and for the same mentionable reasons previously. **Fig.(13)** explains the variation of the mean Nusselt number with buoyancy ratio for different values of Darcy number at $\varepsilon=0.9$, generally it is clear that the minimum rate of heat transfer is at $N=-1$ because of the minimum temperature gradients at that case, after that, heat transfer levels begin to increase with the increase of each one of positive or negative buoyancy ratios, also it is clear that the values of Nusselt number will be lower than them at the same values of positive buoyancy ratio because the thermal and solutal buoyancy effects at negative buoyancy ratios will be in opposite direction while they in same direction at positive buoyancy ratios to form (assisting flow), and finally it was noted that the mean Nusselt number generally increases with Darcy number increase because of the decreasing in overall bed resistance to the flow inside it as a result to the increasing in the volume of passable paths of fluid through the packed bed. **Fig.(14)** explains the variation of the mean Nusselt number with buoyancy ratio for different values of porosity at $Da=10^{-1}$, where it was noted that when porosity equals to a value in the range of $(\varepsilon=0.5\sim0.8)$, the values of mean

Nusselt number will increase gradually with the increase of porosity in that range, but when the porosity increases above that range, the values of mean Nusselt number will decrease, and for explaining this phenomenon clearly we must return to **Eq.(20.a)**, where it is noted that the whole value of local Nusselt number is multiplicand by the porosity while the second term in this equation (solid phase term) was multiplicand by the inverse of dimensionless thermal conductivity $\Lambda^{-1}$ which decreases with the increase of porosity $\left[\Lambda^{-1} = (1-\varepsilon)\, k_s / \varepsilon\, k_f\right]$, so, when the porosity values equal to or less than ***(0.8)***, the value of Nusselt number will increase, while it decreases after that value of porosity because the value of dimensionless thermal conductivity will be very small and it causes decreasing in Nusselt number more than the increasing in it because of porosity. **Fig.(15)** shows the variation of the mean Sherwood number with buoyancy ratio for different values of Darcy number at $\varepsilon=0.9$, where Sherwood number will comport a similar behavior to Nusselt number variation with buoyancy ratio and Darcy number and for the same mentionable reason previously, while **Fig.(16)** explains the variation of the mean Sherwood number with buoyancy ratio for different values of porosity at $Da=10^{-1}$, where it is clear that the values of Sherwood number will increase with increase of packed bed porosity because the flow levels will increase as a result of decreasing in the occupied volume by the bed through enclosure, where the overall packed bed resistance to the flow will decrease. To exhibit the reliability of the presented results, the variation of mean Nusselt number with the buoyancy ratio at $Gr_T \approx 1.4\times10^5$ was compared with results of **(Rahli and Bouhadef, 2004)** as it is shown in **Fig.(17)**, where it is clear the similarity in Nusselt number behavior with the mentionable study, but there is a small difference between these values because of the using of (LTNE) model in the present study which causes more heat transfer due to both the fluid and solid phases.

## CONCLUSIONS

This paper has presented a numerical investigation of double-diffusive flow in a packed bed square enclosure by using local thermal non-equilibrium (LTNE) model, and from the obtained results, the following conclusions are drawn;

1- At the positive buoyancy ratios $N\geq0$, the flow takes the clock wise direction, while at $N=-1$ the flow begins to reverse its direction as it happens at $N<-1$.
2- Generally, levels of flow, heat transfer and mass transfer increase with the increase of both the positive or negative buoyancy ratio as a result of increasing in the total buoyancy effects.
3- The values of Nusselt number increase with increase of Darcy Number.
4- The values of Nusselt number increase with increase of porosity until the porosity reaches a certain value of about ($\varepsilon \approx 0.8$) where the value of mean Nusselt number will decrease after that value of porosity.
5- The values of Sherwood number increase with increase of both Darcy Number and the porosity.

## REFERENCES

A. Amiri and K. Vafai, Transient analysis of incompressible flow through a packed bed, International Journal of Heat and Mass Transfer, 41, 4259-4279, 1998.

A. K. Bukhari, Double diffusive convection in a horizontal porous layer superposed by a fluid layer, Umm Al-Qura Univ. J. Sci. Med. Eng. Vol. 15, No. 2, pp. 95-113, 2003.

I. Hajri*, A. Omri and S. Ben Nasrallah, A numerical model for the simulation of double-diffusive natural convection in a triangular cavity using equal order and control volume based on the finite elements method, Desalination 206, 579-588, 2007.

K. Khanafer and K. Vafai, Double-diffusive mixed convection in a lid-driven enclosure filled with a fluid saturated porous medium, Numerical Heat Transfer, Part A, 42: 465-486, 2002.

M. Mamou, P. Vasseur and M. Hasnaoui, On numerical stability analysis of double-diffusive convection in confined enclosures, J. Fluid Mech., vol. 433, pp. 209-250, 2001.

Md. Shariful Alam, M. M. Rahman and Md. Abdul Maleque, Local similarity solutions for unsteady MHD free convection and mass transfer flow past an impulsively started vertical porous plate with Dufour and Soret effects, Thammasat Int. J. Sc. Tech., Vol. 10, No. 3, July-Sept., 2005.

O. Rahli and K. Bouhadef *, Double-diffusive natural convection in a partially porous square enclosure; effect of the inclination, Laboratoire LTPMP, Faculté de Génie Mécanique et Génie des Procédés, USTHB, Alger – Algérie, 2004.

Q. W. Wang*, M. Zeng, Z. P. Huang, G. Wang, H. Ozoe, Numerical investigation of natural convection in an inclined enclosure filled with porous medium under magnetic field, International Journal of Heat and Mass Transfer 50, 3684-3689, 2007.

R. A. Mohamed, Double-diffusive convection-radiation interaction on unsteady MHD flow over a vertical moving porous plate with heat generation and soret effects, Applied Mathematical Sciences, Vol. 3, no. 13, 629 - 651, 2009.

R. C. Chaudhary and Arpita Jain, Combined heat and mass transfer effects on MHD free convection flow past an oscillating plate embedded in porous medium, Rom. Journ. Phys., Vol. 52, Nos. 5–7, P. 505–524, Bucharest, 2007.

S.C. Saha, M.A. Hossain, Natural convection flow with combined buoyancy effects due to thermal and mass diffusion in a thermally stratified media, Nonlinear Analysis: Modelling and Control, Vol. 9, No. 1, 89–102, 2004.

Versteeg H. K. and Malalasekera W., An introduction to computational fluid dynamics the finite volumes method, Longman Group Ltd, 1995.

Y. Masuda, M. Yonaya, T. Ikeshoji, S. Kimura, F. Alavyoon, T. Tsukada, M. Hozawa, Oscillatory double-diffusive convection in a porous enclosure due to opposing heat and mass fluxes on the vertical walls, International Journal of Heat and Mass Transfer 45, 1365-1369, 2002.

Yoshio Masuda, Michio Yoneya, Akira Suzuki, Shigeo Kimura and Farid Alavyoon, Numerical analysis of double-diffusive convection in a porous enclosure due to opposing heat and mass fluxes on the vertical walls -Why does peculiar oscillation occur?-, Research Center for Compact chemical Process, National Institute of Advanced Industrial Science and Technology, 4-

2-1 Nigatake, Miyagino-ku, Sendai 983-8551, Japan, 2008.

### *Nomenclature*

| | |
|---|---|
| $a$ | side length of the enclosure (m) |
| $a_{sf}$ | specific surface area of the packed bed ($m^{-1}$) |
| $C$ | dimensionless solutal concentration |
| $c$ | solutal concentration (kmol $m^{-3}$) |
| $cp$ | specific heat at constant pressure (J $kg^{-1}$ $K^{-1}$) |
| $D$ | concentration diffusion coefficient ($m^2$ $s^{-1}$) |
| $Da$ | Darcy number |
| $d_p$ | sphere particle diameter (m) |
| $F$ | geometric function |
| $Gr_C$ | solutal Grashof number |
| $Gr_T$ | Grashof number |
| $g$ | gravitational acceleration (m $s^{-2}$) |
| $h_{sf}$ | solid-fluid heat transfer coefficient($Wm^{-2}K^{-1}$) |
| $k$ | thermal conductivity (W $m^{-1}$ $K^{-1}$) |
| $K$ | permeability ($m^2$) |
| $N$ | buoyancy ratio |
| $Nu$ | Nusselt number |
| $p$ | pressure (Pa) |
| $P$ | dimensionless pressure |
| $Pr$ | Prandtl number |
| $Sc$ | Schmidt number |
| $Sh$ | Sherwood number |
| $T$ | temperature (K°) |
| $u, v$ | velocity components (m $s^{-1}$) |
| $U, V$ | dimensionless velocity components |
| $x, y$ | x-, y-coordinates (m) |
| $X, Y$ | dimensionless coordinates |

### *Greek symbols*

| | |
|---|---|
| $\alpha$ | thermal diffusivity ($m^2$ $s^{-1}$) |
| $\mu$ | dynamic viscosity (kg $m^{-1}$ $s^{-1}$) |
| $\nu$ | kinematic viscosity ($m^2$ $s^{-1}$) |
| $\rho$ | density (kg $m^{-3}$) |
| $\beta_T$ | thermal expansion coefficient ($K^{-1}$) |
| $\beta_C$ | solutal expansion coefficient (kmol$^{-1}$ $m^3$) |
| $\theta$ | dimensionless temperature |
| $\psi$ | dimensionless stream function |
| $\omega$ | dimensionless vorticity |
| $\Phi$ | general scalar dependent variable |
| $\Gamma$ | diffusion coeffecient |
| $\varepsilon$ | porosity |
| $\Lambda$ | dimensionless thermal conductivity |
| $\xi$ | dimensionless solid-to-fluid heat transfer coefficient |

### *Subscripts*

| | |
|---|---|
| $f$ | fluid |
| $feff$ | effective properties for fluid |
| $H$ | high |
| $i$ | axis indication |
| $L$ | low |
| $l$ | local value |
| $m$ | mean value |
| $s$ | solid |
| $seff$ | effective properties for solid |

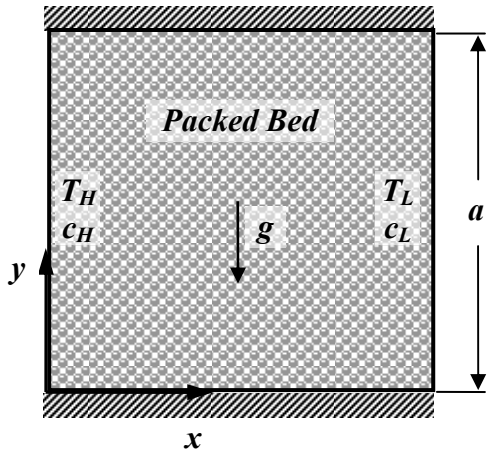


**Fig.(1) schematic diagram of the physical system**

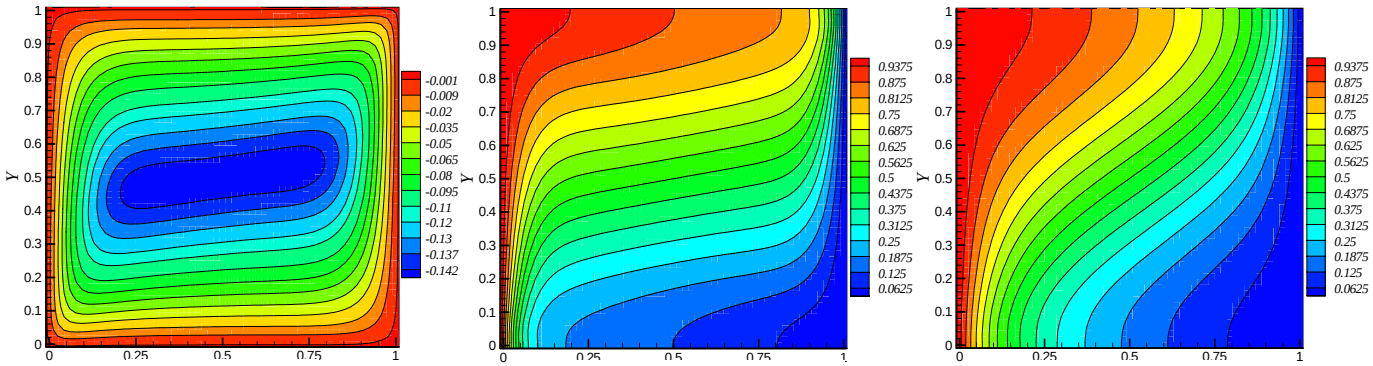


a) Streamlines b) Fluid phase temperature c) Solutal concentration

Fig. (2) Properties distribution at; N=0, $Da=1\times10^{-1}$ & $\varepsilon=0.9$

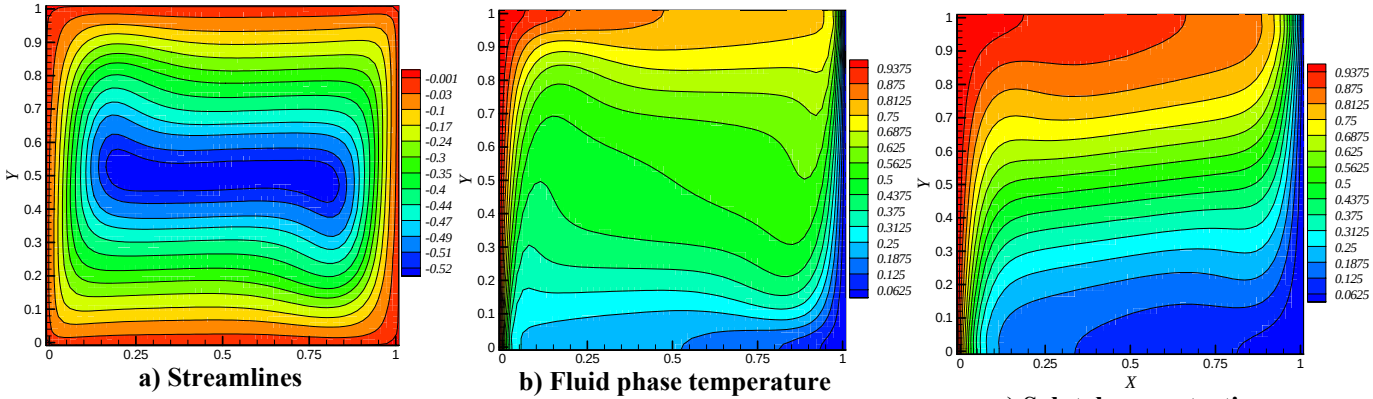


a) Streamlines b) Fluid phase temperature c) Solutal concentration

Fig. (3) Properties distribution at; N=5, $Da=1\times10^{-1}$ & $\varepsilon=0.9$

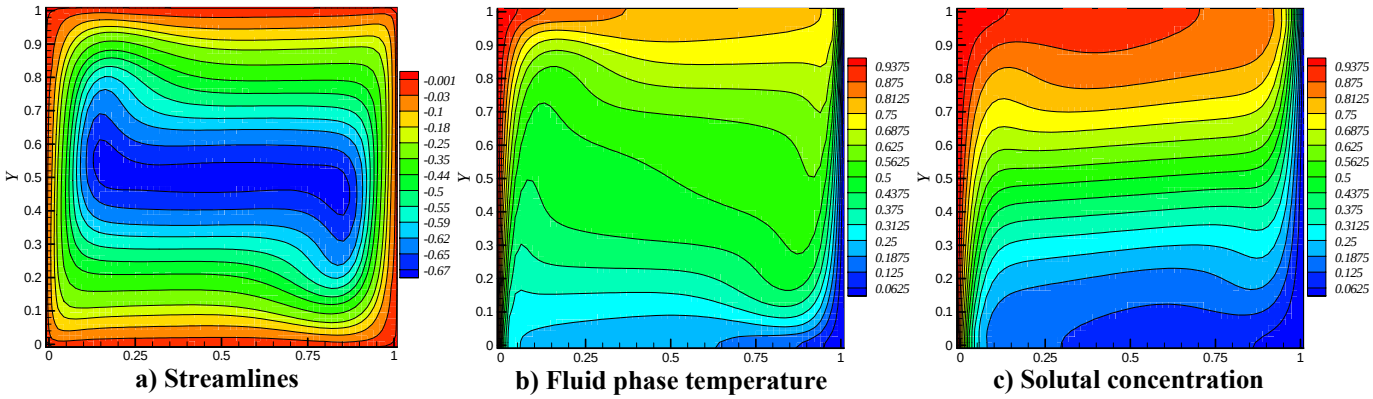


a) Streamlines b) Fluid phase temperature c) Solutal concentration

Fig. (4) Properties distribution at; N=10, $Da=1\times10^{-1}$ & $\varepsilon=0.9$

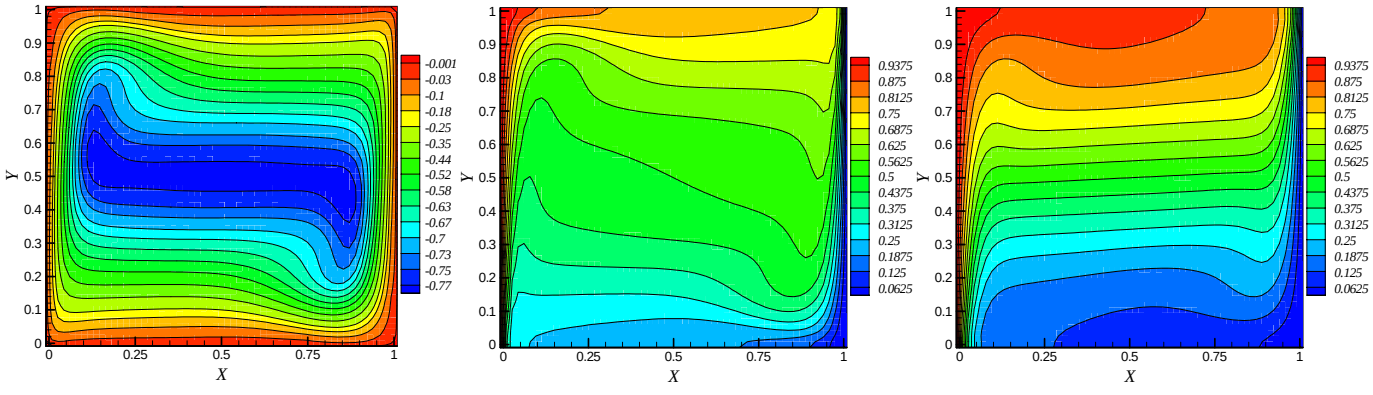


a) Streamlines b) Fluid phase temperature c) Solutal concentration

Fig. (5) Properties distribution at; N=15, $Da=1\times10^{-1}$ & $\varepsilon=0.9$

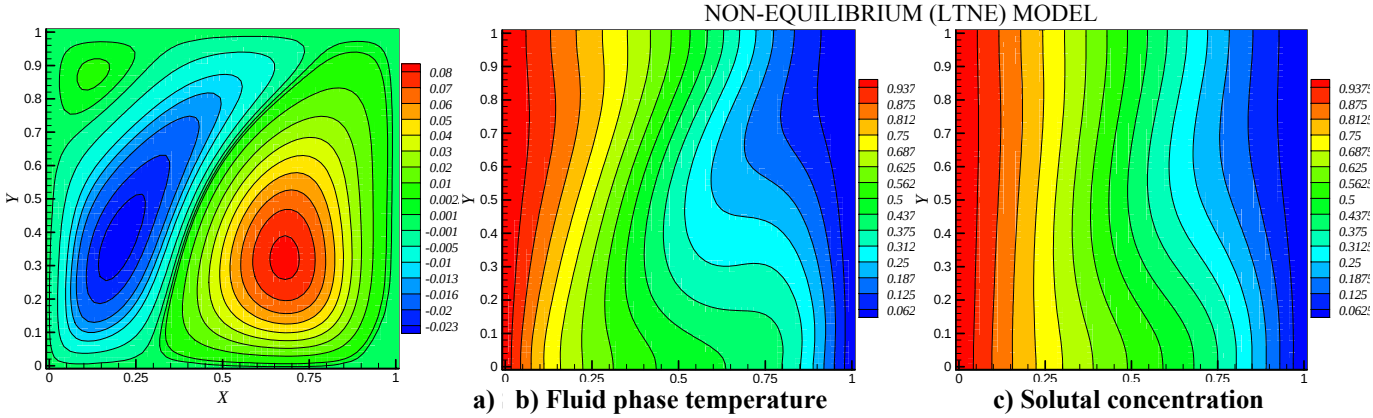


a) b) Fluid phase temperature c) Solutal concentration

**Fig. (6) Properties distribution at; N=-1, Da=1×10$^{-1}$ & ε =0.9**

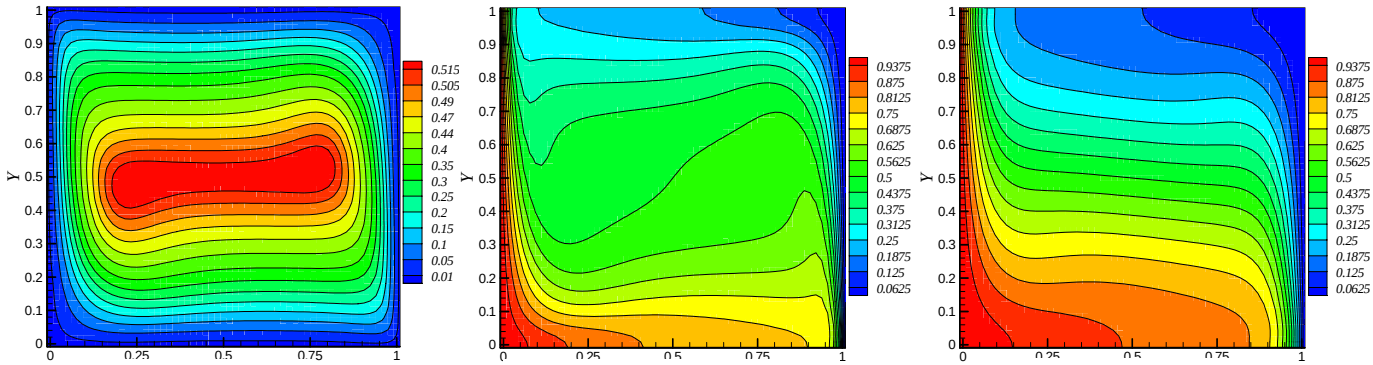


a) Streamlines b) Fluid phase temperature c) Solutal concentration

**Fig. (7) Properties distribution at; N=-5, Da=1×10$^{-1}$ & ε =0.9**

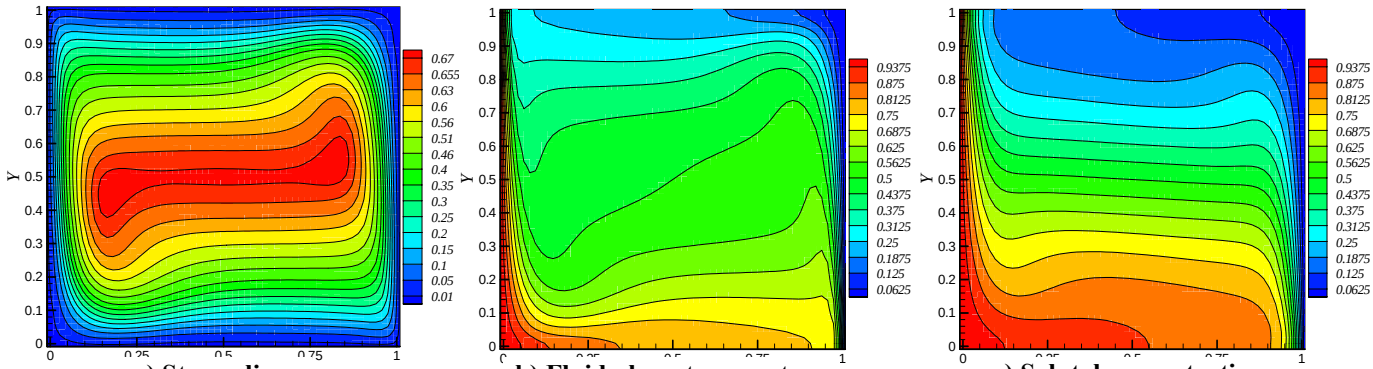


a) Streamlines b) Fluid phase temperature c) Solutal concentration

**Fig. (8) Properties distribution at; N=-10, Da=1×10$^{-1}$ & ε =0.9**

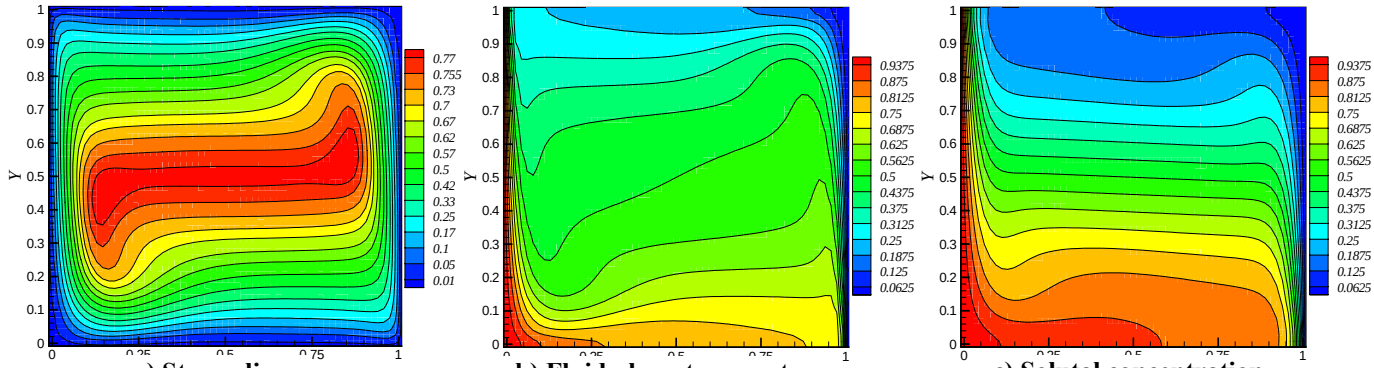


a) Streamlines b) Fluid phase temperature c) Solutal concentration

**Fig. (9) Properties distribution at; N=-15, Da=1×10$^{-1}$ & ε =0.9**

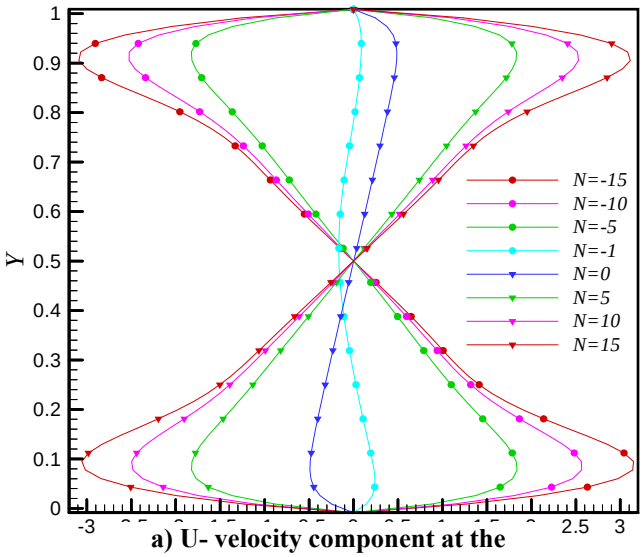


a) U- velocity component at the intermediate vertical location

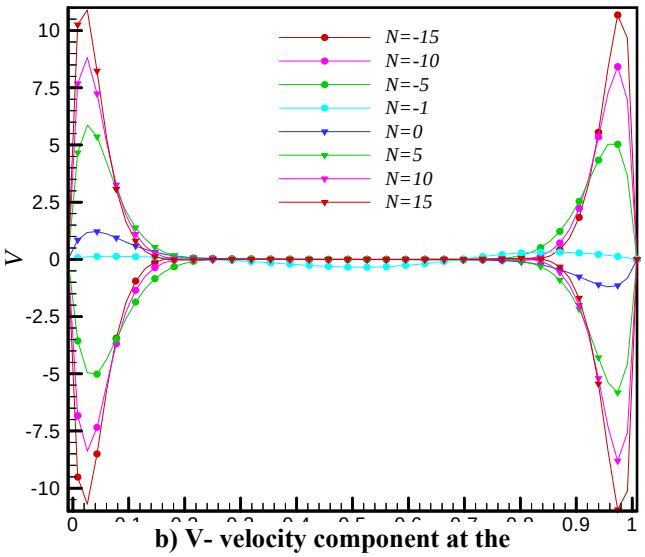


b) V- velocity component at the intermediate horizontal location

**Fig. (10) Variation of velocity components with buoyancy ratio at the intermediate vertical and horizontal locations for Da=1×10$^{-1}$ & ε =0.9**

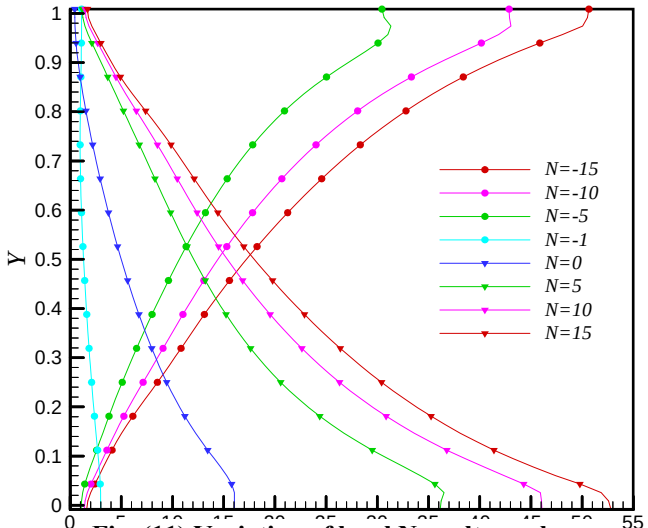


**Fig. (11) Variation of local Nusselt number with buoyancy ratio at ε=0.9 & Da=1×10$^{-1}$**

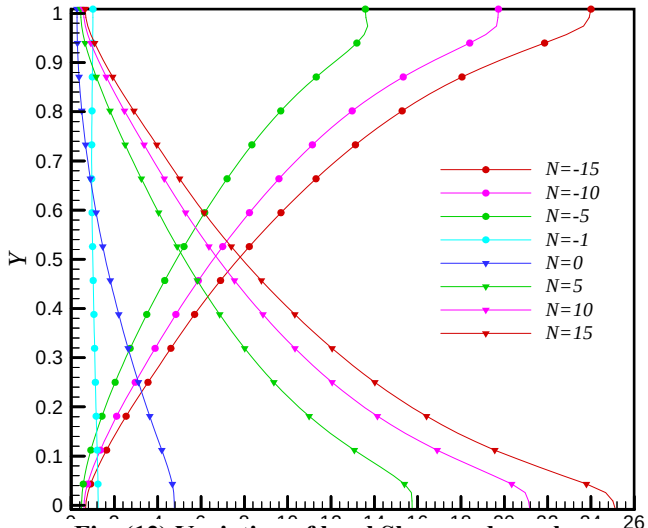


**Fig. (12) Variation of local Sherwood number with buoyancy ratio at ε=0.9 & Da=1×10$^{-1}$**

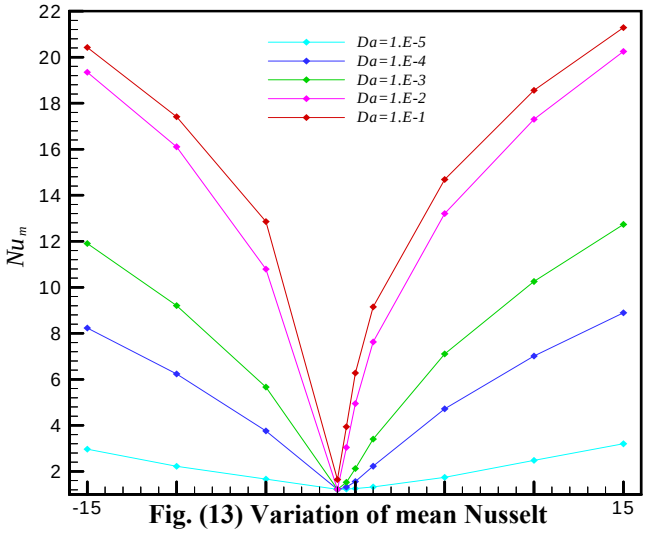


**Fig. (13) Variation of mean Nusselt number with Darcy number at ε=0.9**

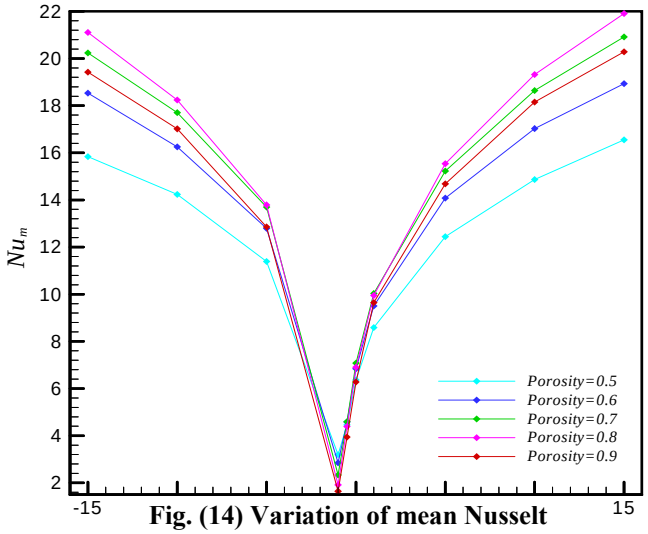


**Fig. (14) Variation of mean Nusselt number with porosity at Da=1.E-1**

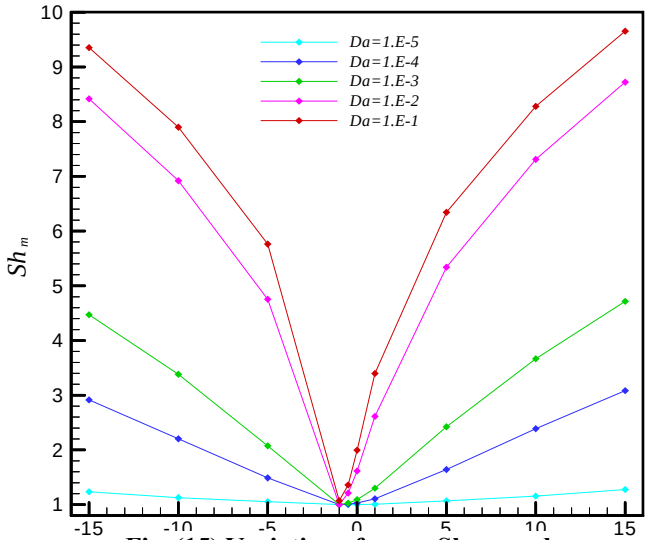


**Fig. (15) Variation of mean Sherwood number with Darcy number at ε=0.9**

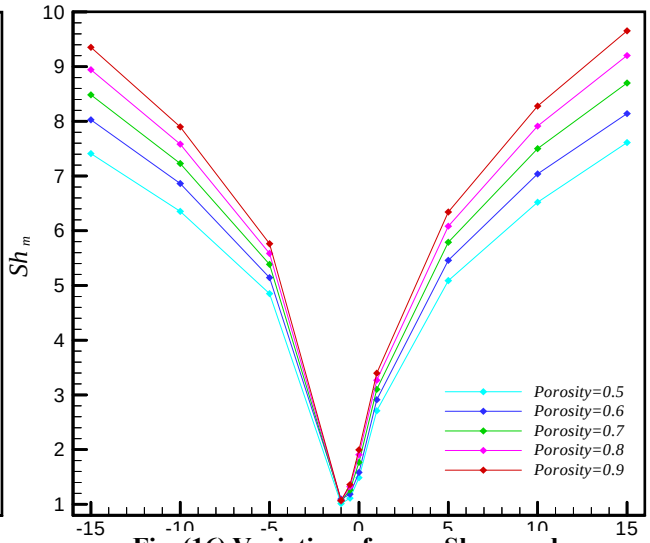


**Fig. (16) Variation of mean Sherwood number with porosity at Da=1.E-1**

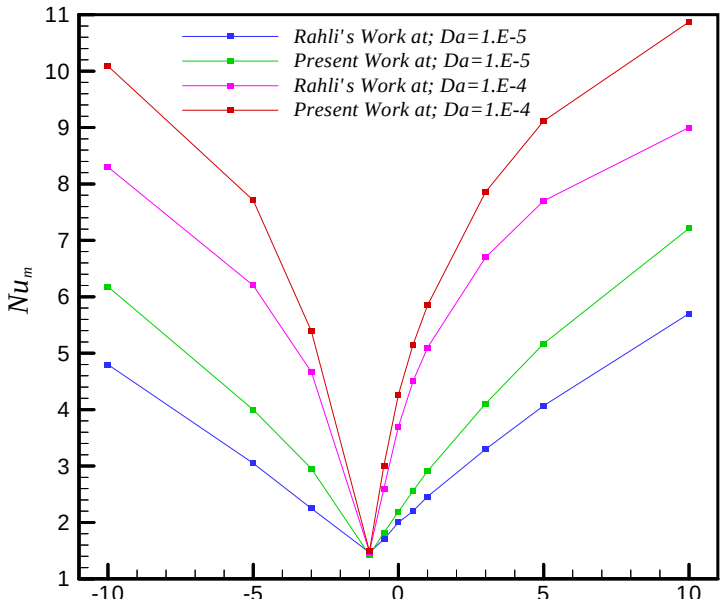


**Fig. (17) Comparison the variation of mean Nusselt number with buoyancy ratio at $Gr_T \approx 1.4\times10^5$ with the work of (Rahli and Bouhadef, (2004)**